# Journal of Materials Chemistry A

Accepted Manuscript


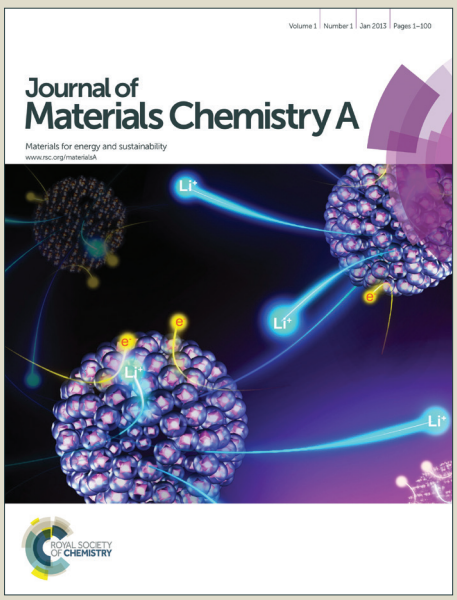





ROYAL SOCIETY OF CHEMISTRY

www.rsc.org/materialsA

Crystalline Cu-Sn-S Framework for High Lithium Storage Performance

Lina Nie, Yu Zhang, Kaiqi Ye, Jianyu Han, Yue Wang, Rakesh Ganguly, Yongxin Li, Rong Xu,* Qingyu Yan,* Qichun Zhang*

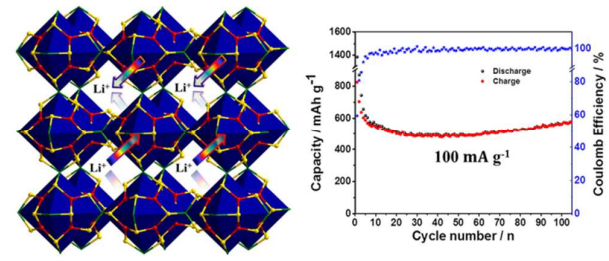


Three-deminsional crystalline $(H_3O)_2(enH_2)Cu_8Sn_3S_{12}$ framework exhibits a high capacity of 563 mA h $g^{-1}$ at a current density of 0.1 A $g^{-1}$ with high stability.

Journal of Materials Chemistry A

ARTICLE

# Crystalline Cu-Sn-S Framework for High-Performance Lithium Storage

Received 00th January 20xx,
Accepted 00th January 20xx

DOI: 10.1039/x0xx00000x

www.rsc.org/

Lina Nie,[abg] Yu Zhang,[bcg] Kaiqi Ye,[e] Jianyu Han,[f] Yue Wang,[e] Rakesh Ganguly,[d] Yongxin Li,[d] Rong Xu*[f], Qingyu Yan,*[b] Qichun Zhang*[bd]

In order to address the increasing demands for clean energy, it is highly desirable to explore new electrode materials to improve the efficiency of lithium ion batteries (LIBs). In this work, we report the successful synthesis of crystalline $(H_3O)_2(enH_2)Cu_8Sn_3S_{12}$ material via surfactant-thermal strategy. The crystal structure analysis shows that the as-prepared chalcogenide has 3D interconnected channels occupied by disordered $H_2en^{2+}$ and $H_3O^+$. Taking advantages of porous structures and $H_2en^{2+}$ and $H_3O^+$ as stabilizers, $(H_3O)_2(enH_2)Cu_8Sn_3S_{12}$ has been explored as anode material for lithium ion batteries. Our result exhibits a high capacity of 563 mA h $g^{-1}$ at a current density of 0.1 A $g^{-1}$ after 100 cycles. In addition, outstanding cycling properties are demonstrated with only 7.2 % capacity loss from 5$^{th}$ to 100$^{th}$ cycle. Our research could provide the insight to the exploration of crystalline ternary thiostannate for lithium ion batteries in the future.

## Introduction

Production and storage of clean and renewable energy have become an urgent and concerned issue over the past decades. Therefore, innovative research has been largely focused on several promising energy storage and supply methods, such as lithium ion batteries (Li: the most electropositive and lightest) [1, 2], sodium ion batteries (Na: abundant and similar chemical properties to Li)[3, 4], magnesium-ion batteries (Mg: the divalent nature and usability of Mg metal anodes )[5-9], metal-air batteries (using oxygen from air as a main reactant)[10-13] and so on. Among these, Li-ion batteries (LIBs) have been dominating the market for portable electronic devices and electric vehicles.[14-18] Normally, the commercial batteries compose of a lithium compound cathode (for example, $LiCoO_2$ or $LiFePO_4$), a graphitic anode and an organic carbonate electrolyte with achieved energy densities of ~ 120-150 Wh $kg^{-1}$.[19] However, a critical bottleneck of LIBs is the low theoretical specific capacity (up to 372 mA h $g^{-1}$) of conventional graphite anodes, which is unable to meet increasing demands for efficient energy.[19, 20] In addition, environmental friendly components are also very important considering the rising awareness of environmental issues. Therefore, many current researches focus on alternative anode materials such as Si (4200 mA h $g^{-1}$),[21-23] Sn (994 mA h $g^{-1}$),[24-26] P (1552 mA h $g^{-1}$)[27-29] and Sb (660 mA h $g^{-1}$)[30, 31]. Unfortunately, their application has been mostly confined by their poor cycling life and severe pulverization due to high volume expansion/contraction of nearly 400% as well as the large irreversible capacity during the repeated lithiation and delithiation process.

Going beyond the limitation of current LIBs requires exploring new electrode materials with optimized structures. The control over the morphology, composition and pore structures of the active materials has been proven to be a promising strategy for their applications in LIBs. In particular, porous materials are attractive because of their accommodation of the volume expansion during the repeated lithiation and delithiation process, large surface-to-volume ratio with the improved contact area between electrode materials and electrolyte, as well as short diffusion length for lithium ions. For example, $FePO_4$ nanoflakes with ordered channels,[32] mesoporous $FeF_3{\cdot}0.33H_2O$,[33] and $Co_3O_4$ nanowall arrays[34] have been used as electrode materials for LIBs and exhibited superior electrochemical properties. Given this, there is still much room for the enhanced performance of LIBs with regard to the development of nanostructures for their potential energy applications.[35-37]

Tin-based materials have been regarded as the most attractive candidates of anode materials for LIBs with a higher capacity (> 600 mA h $g^{-1}$) compared with that of the commercial graphite electrode.[38-40] Among them, tin sulfides have attracted great attention owing to their high theoretical capacity, natural abundance and low toxicity.[41-43] However, their long-term cycling properties are still far from satisfactory. I–III–VI and I–IV–VI series of tin-based ternary sulfides semiconducting materials, including Ag-

[a] Nanyang Environment and Water Research Institute, Interdisciplinary Graduate School, Nanyang Technological University, Singapore 639798, Singapore.
[b] School of Materials Science and Engineering, Nanyang Technological University, Singapore 639798, Singapore.
[c] Energy Research Institute @NTU, Interdisciplinary Graduate School, Nanyang Technological University, Singapore 639798, Singapore.
[d] Division of Chemistry and Biological Chemistry, School of Physical and Mathematical Sciences, Nanyang Technological University, Singapore 637371, Singapore.
[e] State Key Laboratory of Supramolecular Structure and Materials, College of Chemistry, Jilin University, Changchun 130012, PR China.
[f] School of Chemical and Biomedical Engineering, Nanyang Technological University, Singapore 637459, Singapore
[g] These authors contributed equally to this work.
† Footnotes relating to the title and/or authors should appear here.
Electronic Supplementary Information (ESI) available: [details of any supplementary information available should be included here]. See DOI: 10.1039/x0xx00000x

Sn-S,[44] $Cu_3SnS_4$,[45] and $Cu_2SnS_3$[46] have drawn much attention due to their wide applications in photocatalytic activity for hydrogen evolution, photovoltaic devices and so on. Unlike those extensively studied transition metal oxides[47-49] or sulfides,[50-52] the investigation of ternary thiostannates as anode materials for lithium ion batteries have not been paid much attention.

In this work, we report on the successful synthesis of 3D-$(H_3O)_2(enH_2)Cu_8Sn_3S_{12}$ single crystals through surfactant-thermal method[53-58] and the exploration of its promising energy application as anode materials for LIBs. In its structure, 3D interconnected channels are highly ordered, in which disordered $H_2en^{2+}$ and $H_3O^+$ are located. It is expected that the highly porous structure is beneficial for good electrolyte penetration and also fast de/lithiation process.[59-61] In addition, organic small molecules are proposed to serve as stabilizers to avoid structure collapse as frequently reported in the field of battery materials (e.g., oxide and phosphate cathode).[33, 62-64] More importantly, when evaluated as the electrode material for lithium-ion batteries, $(H_3O)_2(enH_2)Cu_8Sn_3S_{12}$ delivered a specific capacity of 563 mA h $g^{-1}$ at a current density of 0.1 A $g^{-1}$ after 100 cycles as well as outstanding cycling properties with only 7.2 % capacity loss from 5$^{th}$ to 100$^{th}$ cycles. This investigation will open up a new exploration of ternary thiostannate single crystals for lithium ion batteries in the future.

## Experimental section

All chemicals were commercially available and used without further purification. The scanning electron microscope (SEM) image and elemental analyses of Cu, Sn and S were performed on an EDX-equipped JEOL/JSM-6360A SEM. Transmission electron microscopy (TEM) images were taken with JEOL 2100F at 200 kV. Elemental analyses (N, C, H) were performed on an Elementary Vario El III instrument. Sample weight is typically 5 mg and accuracy up to 5%. Powder X-ray diffraction data were recorded on a Bruker D8 Advance diffractometer with a graphite-monochromatized Cu $K_\alpha$ radiation. The data were collected with 2$\theta$ in a range of 5°-65°. The FT-IR spectra (KBr pellets) were recorded on a PerkinElmer FTIR spectrophotometer in the range 500−4000 $cm^{-1}$. Thermal stability study was carried out on a TGA Q500 instrument under flowing $N_2$ with a heating rate of 10°C /min up to 450°C.

The precursor $Na_4SnS_4{\cdot}14H_2O$ was synthesized through a solution reaction. Firstly, 60 mmol $Na_2S{\cdot}9H_2O$ was dissolved in 50 mL of $H_2O$ with stirring. Then 15 mmol of $SnCl_4$ was diffused in 25 mL $H_2O$ and added dropwise with continuous stirring. The immediately formed yellow precipitates would be dissolved with stirring and the mixture became greenish liquid. It was stirred at 45 ℃ for 15 h and then added to 200 mL methanol and stored in refrigerate for 24 h.

**Synthesis of $(H_3O)_2(enH_2)_2Cu_8Sn_3S_{12}$ (denoted as CTS).**

A mixture of $Cu_2S$ powder (0.25 mmol, 40 mg), $Na_4SnS_4{\cdot}14H_2O$ (0.25 mmol, 147 mg), S (1.00 mmol, 32 mg), ethylenediamine (99.5 %, 2.0 ml), and octylamine (99 %, 2.0 ml) was sealed into an autoclave equipped with a Teflon liner (20 ml) and heated at 160 °C for 6 days. After cooling to room temperature, the mixture was washed with ethanol and black polyhedron crystals of CTS were obtained by filtration and selected by hand (yield: 49 % based on Cu). Elemental analysis (EA) for compounds CTS, Calcd, N: 2.075, C: 1.779, H: 1.186; Found, N: 2.126, C: 2.332, H: 1.238. CCDC number: 1408735.

**Single crystal X-ray crystallography**

The single crystal X-ray diffraction data were collected on a Bruker APEX II CCD diffractometer with a graphite-monochromatized Mo-Kα radiation source (λ = 0.71073 Å). The structure was solved by direct methods and refined by full-matrix least-squares cycles in SHELX-97.[65] Because of the disorder of protonated ethylenediamine and water in CTS, it was impossible to locate them in the final structural refinement. The relevant crystallographic data and structure refinement details are listed in Table S1.

**Electrochemical measurements**

The as-prepared products were first grinded for about 10 minutes. For the electrode preparation, 70 wt% of the as-prepared active materials, 20 wt% active carbons, and 10 wt% polyvinylidene fluoride (PVDF) binder were mixed with N-methyl-2-pyrrolidinone (NMP). The slurry was coated onto Cu foil used as working electrodes. Then they were dried in a vacuum oven at 50 °C for 12h. Electrochemical measurements were carried out on CR2032 coin-type cells with lithium metal as the counter/reference electrode, a Celgard 2400 membrane as the separator, and 1 M LiPF6 dissolved in a mixture of ethylene carbonate (EC) and dimethyl carbonate (DMC) (EC/DMC, 1: 1, v/v). The coin cells were assembled in an Ar-filled glove box with concentrations of moisture and oxygen below 0.1 ppm. The charge-discharge tests were performed with a NEWARE battery tester at a voltage window of 0.01-3.0 V. Cyclic voltammetry (0.01-3V, 0.1 mV $s^{-1}$) was carried out on Solartron analytical equipment (Model 1470E).

## Results and discussion

Although there are lots of methods such as high-temperature solid-state synthesis, solution process, hydro(solvo)thermal synthesis, and ionthermal synthesis to prepare chalcogenids,[66-71] we are more interested in surfactant-thermal method due to the special characteristics of surfactants, such as thermal stability, the cheap price and multifunctional properties. Acting as structure-directing agents, surfactants could control the pore sizes and phases of crystalline zeolite frameworks.[72] Moreover, surfactants have more power to produce high-quality crystals due to their viscosity.

The purity and stability of CTS have been examined by PXRD and TGA. The amounts of protoned water and ethylenediamines were confirmed by elemental analysis and TGA analysis. The results are provided in supporting information.

**Structure of $(H_3O)_2(enH_2)_2Cu_8Sn_3S_{12}$**

Single crystal X-ray diffraction (XRD) analysis revealed that CTS crystallizes in the cubic space group *F*-43*c* and contains a 3D anionic open-framework $[Cu_8Sn_3S_{12}]^{4-}$ with disordered $H_2en^{2+}$ and $H_3O^+$ located in the channels as charge-balanced species.

Figure 1a shows the scanning electron microscopy (SEM) image of the as-prepared sample. As demonstrated in Figure 1c, a d-spacing of 0.285 nm in High-resolution transmission electron microscopy (HRTEM) image can be obtained, corresponding to the (026) plane. This plane can be indexed to the powder XRD (Figure 1b) peak centered at 31.34°. The selected-area electron diffraction (SAED) pattern (Figure 1d) reveals the high degree of crystallinity of the products. Clearly, it shows the product belongs to the cubic system.

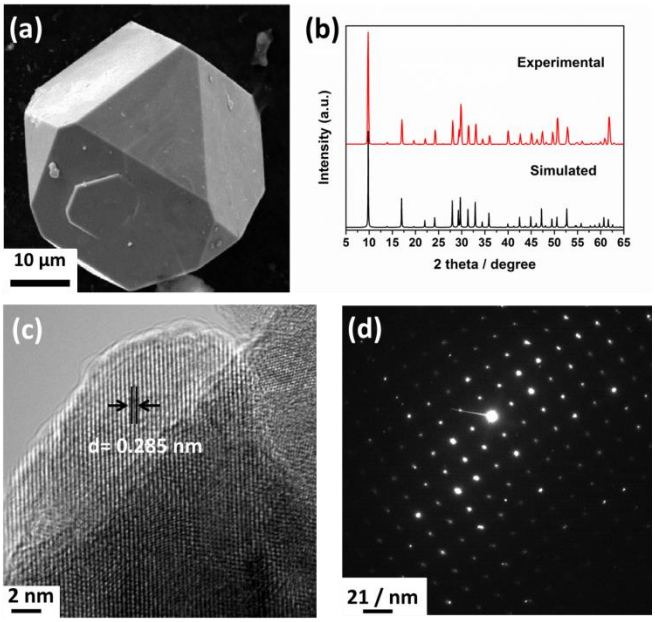


**Figure 1**. Characterization of CTS. (a) SEM image; (b) XRD pattern; (c) High-resolution TEM image; (d) SAED pattern.

In the asymmetric unit of CTS, Cu1 and Cu2 adopt $[CuS_3]$ planar trigonal geometries by coordinating to three $\mu_3$-$S^{2-}$ ions. The Cu-S bond lengths range from 2.253(7) to 2.257(7) Å that are consistent with the values in the similar structures.[73-75] Sn1 is tetrahedrally coordinated by four $\mu_3$-$S^{2-}$ ions with the Sn-S bond length of 2.4012(18) Å. Each $\mu_3$-$S^{2-}$ ion bridges two Cu (Cu1 and Cu2) sites and one Sn (Sn1) center.

The crucial building block of three-dimensional CTS is icosahedral $[Cu_8S_{12}]^{16-}$ cluster (Figure 2), which consists of a cubic array of eight $Cu^+$ ions bridged by $\mu_3$-$S^{2-}$ ions, and the icosahedral shape is defined by twelve bridging $\mu_3$-$S^2$ ions. The adjacent $[Cu_8S_{12}]^{16-}$ clusters are linked by discrete $Sn^{4+}$ ions, which makes them behave like superoctahedral units, to give rise to a Cu-Sn-S framework with 3D channels (Figure 3).

Interestingly, 3D anionic open frameworks $[Cu_8Ge_5S_{16}]^{4-}$ (**1**),[73] $[Cu_8Ge_4S_{14}]^{4-}$ (**2**) [75] and $[Cu_8Ge_3S_{12}]^{4-}$ (**3**) [74] are also constructed with the icosahedral $[Cu_8S_{12}]^{16-}$ clusters as building blocks. In compound **1**, the icosahedral $[Cu_8S_{12}]^{16-}$ clusters are linked by the dimeric $[Ge_2S_2]^{4+}$ units in *a* and *b* directions, and $Ge^{4+}$ ions in *c* direction, with disordered protonated amines located in the 3D channels. While in **2**, the icosahedra are linked by $[Ge_2S_2]^{4+}$ units in *a* direction and $Ge^{4+}$ sites in *b* and *c* directions. In compound **3**, the icosahedral $[Cu_8S_{12}]^{16-}$ clusters are linked by discrete $Ge^{4+}$ sites in three directions, while in CTS the linkers are $Sn^{4+}$ ions.

It is worth mentioning that although CTS and 3D-$(H_2en)_2Cu_8Sn_3S_{12}$ (**4**) [76] have the same formula of the anionic open-framework $[Cu_8Sn_3S_{12}]^{4-}$ with protonated ethyleneamines as charge balance agents, their structural characteristics are obviously different: a) in CTS, the icosahedral $[Cu_8S_{12}]^{16-}$ clusters are linked by $Sn^{4+}$ ions. In compound **4,** the icosahedra are cross-linked through $[Cu_8S_{16}]^{24-}$ clusters, which the $Sn^{4+}$ ions are incorporated into; b) in CTS, there is only a single channel system, while compound **4** possesses two interpenetrating channel systems along <100> directions and two interpenetrating channel systems along <110> directions.

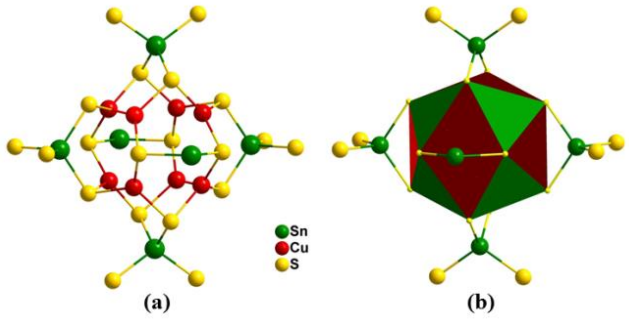


**Figure 2**. Icosahedral $[Cu_8S_{12}]^{16-}$ cluster and its connectivity with six $Sn^{4+}$ ions: (a) Ball and stick mode and (b) polyhedral mode.

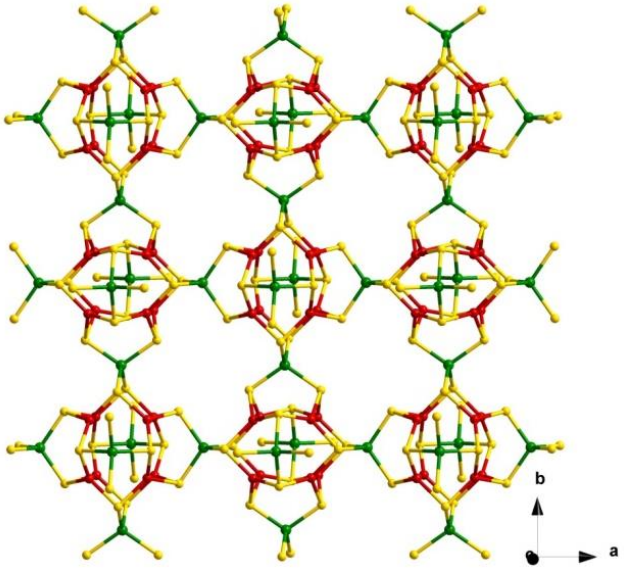


**Figure 3**. View of the 3-D Cu–Sn–S framework along *bc* direction

### Electrochemical Lithium-Storage Performance

With the aim of exploring the potential application of CTS for lithium ion batteries, we evaluated the electrochemical performance with various electrochemical measurements. Figure 4a shows the typical cyclic voltammertry (CV) curves at room temperature (RT) during first 3 cycles (0.01-3V, 0.1 mV $s^{-1}$). For the first cathodic scan, one sharp peak located at 1.54 V, the second broad one at 1.05 V and a small peak at 0.35 V are observed. These peaks can be related to the phase transformation, the decomposition of CTS into Cu and Sn embedded in a $Li_2S$ matrix, and the formation of $Li_xSn$ alloy, respectively.[77] For the first anodic

scan, two broad peaks at 0.56 V and 1.25 V and a sharp one at 1.9 V companied by one at 2.1V are found. The oxidation peak at 0.56 V is known to represent the delithiation process of $Li_xSn$ alloy.[78-80] The other three anodic peaks can be attributed to the continuous oxidation of Cu and Sn. During the subsequent cycles, two new cathodic peaks at 1.56 V and 1.64 V appeare because of some irreversible reactions. The shape of CV curves can almost retain indicating the good stability of the electrochemical process. As the galvanostatic charge-discharge curves also provide detailed information on electrochemical activity, we illustrated the discharge/charge curves for 1st, 2nd, 3rd, 5th and 100th cycles in a voltage range of 0.01-3.0 V (Figure 4b). As can be seen, discharge capacity (1385 mAh $g^{-1}$) and subsequent charge capacity (870.3 mAh $g^{-1}$) show a large initial reversible capacity. In addition, the potential plateaus observed are in good agreement with the redox peaks in the CV curves.

Rate performance of the CTS electrode at both RT and 50 °C was further examined by first cycling the cell at 0.1 A $g^{-1}$ for five cycles with a gradual increase of the discharge/charge rates to as high as 10 A $g^{-1}$, as shown in Figure 4c. The outstanding reversibility of the electrode can be deduced from the almost 100 % coloubic efficiency of each cycle at both room temperature and 50 °C, respectively**.** Reversible capacities at (at RT) of about 800 mAh $g^{-1}$ at a discharge/charge rate of 0.1 A $g^{-1}$, 650 mAh $g^{-1}$ at 0.2 A $g^{-1}$, 520 mAh $g^{-1}$ at 0.5 A $g^{-1}$, 430 mAh $g^{-1}$ at 1 A $g^{-1}$, 215 mAh $g^{-1}$ at 5 A $g^{-1}$, 108 mAh $g^{-1}$ at 10 A $g^{-1}$ are achieved, respectively. It should be noted that a capacity of 623 mAh $g^{-1}$ at 0.1 A $g^{-1}$ can still be achieved after intensive cycles. In addtion, notable capacities at evaluated temperature (50 °C) can also be obtained-- about 500 mAh $g^{-1}$ at 0.1 A $g^{-1}$, 410 mAh $g^{-1}$ at 0.2 A $g^{-1}$, 350 mAh $g^{-1}$ at 0.5 A $g^{-1}$, 283 mAh $g^{-1}$ at 1 A $g^{-1}$, 181 mAh $g^{-1}$ at 5 A $g^{-1}$, 88 mAh $g^{-1}$ at 10 A $g^{-1}$. After intensive cycles, 453 mAh $g^{-1}$ at 0.1 A $g^{-1}$ can also be got. The high reversible capacities at both room temperature and 50 °C indicates the excellent rate performance of the CTS. Hence, we can resonably infer that the excellent rate performance of the CTS proves both the large lithium ion storage and good kinetics, arising from not only the enhanced contact areas between the active materials and electrolyte but also the short lithium ions pathways due to the overall 3D nano-channels distribution in the CTS structures.

The long-term cycling properties of the CTS at both RT and 50 °C were also characterized with a current density of 0.1 A $g^{-1}$ as shown in Figure 4e. One can see that CTS undergoes a capacity drop during the initial cycles (1st to 5th cycle) at both temperatures. The capacity drop is commonly observed in previous studies of transition metal oxides or sulfides as anode materials for LIBs,[81] which could be due to some irreversible reactions at the beginning. During the following cycles, good stability at room temperature can be observed with only 7.2% capacity drop after even 100 cycles. Remarkably, although relatively low capacities compared with those at RT are obtained at evaluated temperature(50 °C), CTS still shows good stability with 91.8% retaiment from 6th to 100th cycle. The good performance at both room temperature and evaluated temperature demonstrats its promising application of lithium ion batteries with long cycling life. The good cycling performance is comparable to or even better than those reported in previous literatures (see a complete list in Table S1 in the Supporting Information).This is possibly due to the unique structure of 3D open framework, which is able to accommodate large volume change along with the redox reactions. Thus the possibility of structure collapse can be reduced significantly.

To gain insight into the reason that single crystals CTS with unique 3D open framework possessed such good cycling performance as electrode materials for LIBs, electrochemical impedance spectroscopy (EIS) was further performed at equilibrium open circuit potential (≈ 0 V). Figure 4d shows the Nyquist spectra of the electrode materials before and after cycling in the frequency range of 100 kHz to 100 mHz, respectively. In impedance spectroscopy, high frequency activity was attributed to charge transfer phenomenon, whereas the low frequency region is ascribed to the mass transfer process. In order to quantify these respective values, a theoretical equivalent circuit of Rs(Q(RctZw)) is used to fit the experimental data, where Rs is the ohmic resistance; Rct is the charge transfer resistance; Q is the double layer capacitance and Zw is the Warburg impedance. With fitting method, Rct of before (203Ω) and after (272Ω) cycling can be obtained. A slight increase of Rct indicates negligible decay of charge transfer kinetics, further revealing the good cycling properties of CTS as potential anode materials for LIBs.

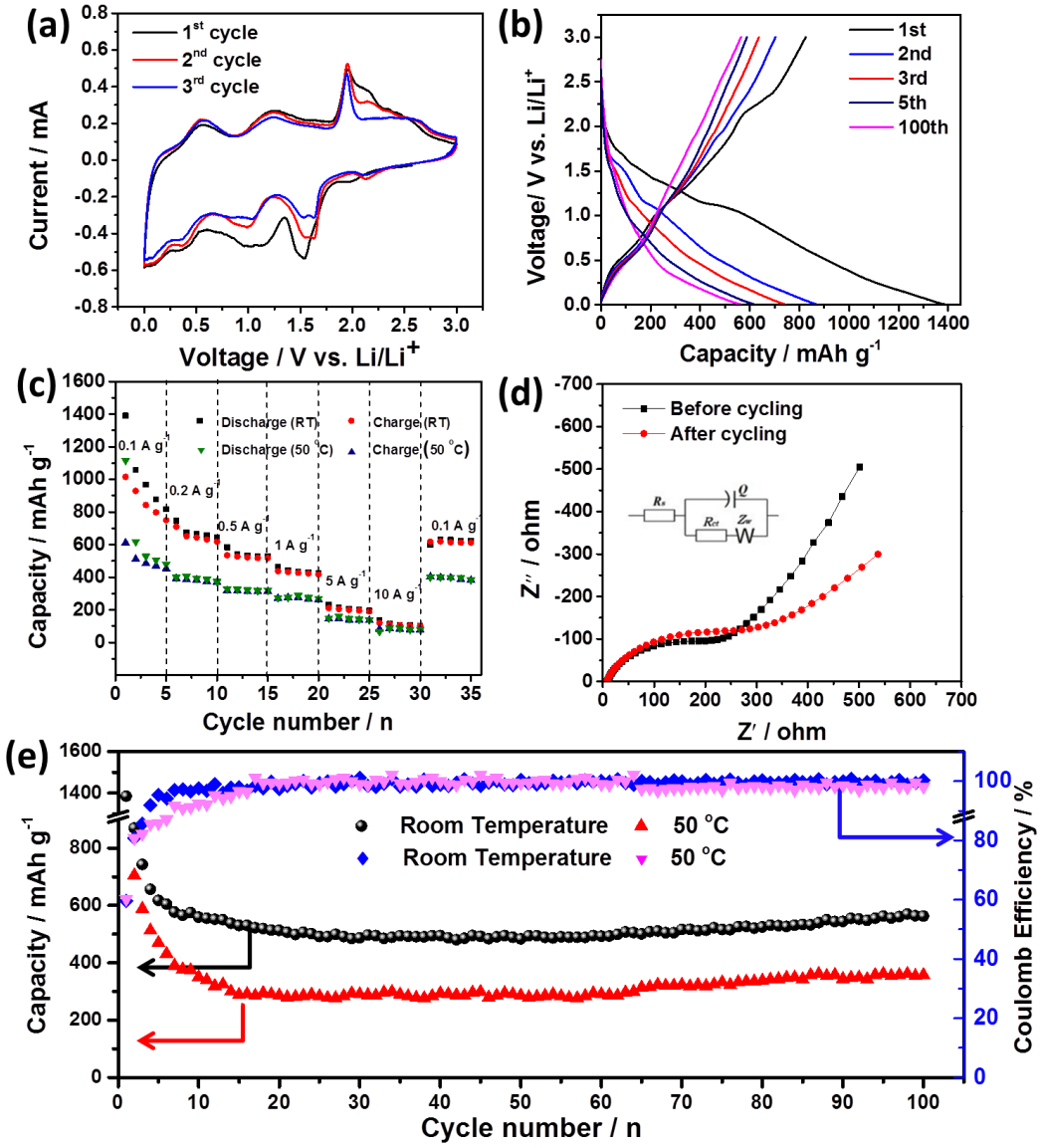


**Figure 4**. Electrochemical characterization of CTS anode. (a) Cyclic voltammograms between 0.01 and 3.0 V measured at a scan rate of 0.1 mV $s^{-1}$; (b) the charge and discharge curves of CTS at a current density of 0.1 A $g^{-1}$; (c) rate performance at different rates; (d) Nyquist plots of CTS electrode before and after cycles, respectively. The inset is the equivalent circuit; (e) capacity as a function of cycle numbers at a current density of 0.1 A $g^{-1}$.

Journal of Materials Chemistry A

ARTICLE

## Conclusion

In summary, we have successfully synthesized the 3D-$(H_3O)_2(enH_2)Cu_8Sn_3S_{12}$ single crystal with interconnected micro-channels (diameter of 1 nm) overall distributed and both of $H_2en^{2+}$ and $H_3O^+$ located in the micro-channels. This structure is very favorable for good electrolyte penetration and fast de/lithiation process as well as good accommodation ability for volume expansion. In addition, $H_2en^{2+}$ and $H_3O^+$ can serve as useful stabilizers to avoid structure collapse. Therefore, when explored as electrode materials for lithium ion batteries, it exhibits outstanding electrochemical performance with a high capacity of 563 mA h $g^{-1}$ at a current density of 0.1 A $g^{-1}$ after 100 cycles as well as good cycling properties with only 7.2 % capacity loss from 5$^{th}$ to 100$^{th}$ cycle. This exploration can open up a new future of ternary thiostannate single crystal for lithium ion batteries.

## Associated content

*Supporting Information

Crystallographic data and structure refinement, EDS, FT-IR, and TGA for CTS; The Supporting Information is available free of charge on the ACS Publications website at DOI: 10.1021/acs.chemmater.

## Author information

Corresponding Author

*E-mail: qczhang@ntu.edu.sg; alexyan@ntu.edu.sg; RXU@ntu.edu.sg.

Notes

The authors declare no competing financial interest.

## Acknowledgements

Q.Z. acknowledges financial support from AcRF Tier 1 (RG 16/12 and RG133/14) and Tier 2 (ARC 20/12 and ARC 2/13) from MOE, and the CREATE program (Nanomaterials for Energy and Water Management) from NRF, Singapore. Q.Z. also thanks the support from Open Project of State Key Laboratory of Supramolecular Structure and Materials (Grant number: sklssm2015027), Jilin University, China.

## Notes and references

1. M. Armand and J. M. Tarascon, *Nature,* 2001**, 414**, 359-367.
2. V. Etacheri, R. Marom, R. Elazari, G. Salitra, D. Aurbach, *Energy Environ. Sci.*, 2011, **4**, 3243-3262.
3. M. D. Slater, D. Kim, E. Lee, C. S. Johnson, *Adv. Func. Mater.,* 2013, **23**, 947-958.
4. S. W. Kim, D. H. Seo, X. Ma, G. Ceder, K. Kang, *Adv. Energ. Mater.*, 2012, **2**, 710-721.
5. Canepa, P., Gautam, G. S., Malik, R., Jayaraman, S., Rong, Z., Zavadil, K. R., Persson, K., Ceder, G., *Chem. Mat.*, 2015, **27**, 3317-3325.
6. R. V. Noorden, *Nature,* 2014, **507**, 26-28.
7. H. D. Yoo, I. Shterenberg, Y. Gofer, G. Gershinsky, N. Pour, D. Aurbach, *Energy Environ. Sci.*, 2013, **6**, 2265-2279.
8. J. Muldoon, C. B. Bucur, T. Gregory, *Chem. Rev.,* 2014, **114**, 11683-11720.
9. M. Liu, Z. Rong, R. Malik, P. Canepa, A. Jain, C. Ceser. K. Persson, *Energy Environ. Sci.,* 2015, **8**, 964-974.
10. F. Cheng, J. Chen, *Chem. Soc. Rev.,* 2012, **41**, 2172-2192.
11. J. S. Lee, S. Tai Kim, R. Cao, N.S. Choi, M Liu,. K. T. Lee, J. Cho, *Adv. Energ. Mater.,* 2011, **1**, 34-50.
12. A. Kraytsberg, Y. Ein-Eli, *J. Power Sources,* 2011, **196**, 886-893.
13. M. A. Rahman, X. Wang, C. Wen, *J. Electrochem. Soc.,* 2013, **160**, A1759-A1771.
14. M. Armand and J. M. Tarascon, *Nature*, 2008, **451**, 652-657.
15. J. Zhu, Z. Yin, D. Yang, T. Sun, H. Yu, H. E. Hoster, H. H. Hng, H. Zhang and Q. Yan, *Energy Environ. Sci.*, 2013, **6**, 987-993.
16. J. Wu, X. Rui, C. Wang, W. B. Pei, R. Lau, Q. Yan and Q. Zhang, *Adv. Energ. Mater.*, 2015, **5**, 1402189.
17. H. Wang, L. F. Cui, Y. Yang, H. S. Casalongue, J. T. Robinson, Y. Liang, Y. Cui and H. Dai, *J. Am. Chem. Soc.*, 2010, **132**, 13978-13980.
18. J. Wu, X. Rui, G. Long, W. Chen, Q. Yan, and Q. Zhang, *Angew. Chem. Int. Ed*, 2015, **54**, 7354–7358.
19. J. Hassoun, F. Bonaccorso, M. Agostini, M. Angelucci, M. G. Betti, R. Cingolani, M. Gemmi, C. Mariani, S. Panero, V. Pellegrini and B. Scrosati, *Nano Lett.*, 2014, **14**, 4901-4906.
20. G. Zheng, Y. Yang, J. J. Cha, S. S. Hong and Y. Cui, *Nano Lett.*, 2011, **11**, 4462-4467.
21. H. Wu and Y. Cui, *Nano Today*, 2012, **7**, 414-429.
22. J. Deng, H. Ji, C. Yan, J. Zhang, W. Si, S. Baunack, S. Oswald, Y. Mei and O. G. Schmidt, *Angew. Chem. Int. Ed.,* 2013, **52**, 2326-2330.
23. J. Ji, H. Ji, L. L. Zhang, X. Zhao, X. Bai, X. Fan, F. Zhang and R. S. Ruoff, *Adv. Mater.*, 2013, **25**, 4673-4677.
24. Y. Xu, Q. Liu, Y. Zhu, Y. Liu, A. Langrock, M. R. Zachariah and C. Wang, *Nano Lett.*, 2013, **13**, 470-474.
25. Z. Wen, S. Cui, H. Kim, S. Mao, K. Yu, G. Lu, H. Pu, O. Mao and J. Chen, *J. Mater. Chem. A*, 2012, **22**, 3300-3306.
26. X. L. Wu, Y. G. Guo and L. J. Wan, *Chem. Asian J.*, 2013, **8**, 1948-1958.
27. L. Q. Sun, M. J. Li, K. Sun, S. H. Yu, R. S. Wang and H. M. Xie, *J. Phys. Chem. C*, 2012, **116**, 14772-14779.
28. Y. Kim, Y. Park, A. Choi, N. S. Choi, J. Kim, J. Lee, J. H. Ryu, S. M. Oh and K. T. Lee, *Adv. Mater.*, 2013, **25**, 3045-3049.
29. W. Li, Z. Yang, Y. Jiang, Z. Yu, L. Gu and Y. Yu, *Carbon*, 2014, **78**, 455-462.
30. A. Darwiche, C. Marino, M. T. Sougrati, B. Fraisse, L. Stievano and L. Monconduit, *J. Am. Chem. Soc.*, 2012, **134**, 20805-20811.
31. W. J. Zhang, *J. Power Sources*, 2011, **196**, 13-24.
32. D. Yang, Z. Lu, X. Rui, X. Huang, H. Li, J. Zhu, W. Zhang, Y. M. Lam, H. H. Hng, H. Zhang and Q. Yan, *Angew. Chem. Int. Ed.*, 2014, **53**, 9352-9355.
33. C. Li, L. Gu, J. Tong, S. Tsukimoto and J. Maier, *Adv. Func. Mater.*, 2011, **21**, 1391-1397.
34. J. Zhu, Y. K. Sharma, Z. Zeng, X. Zhang, M. Srinivasan, S. Mhaisalkar, H. Zhang, H. H. Hng and Q. Yan, *J. Phys. Chem. C*, 2011, **115**, 8400-8406.

35. V. Etacheri, R. Marom, R. Elazari, G. Salitra and D. Aurbach, *Energy Environ. Sci.*, 2011, **4**, 3243-3262.
36. M. G. Kim and J. Cho, *Adv. Func. Mater.*, 2009, **19**, 1497-1514.
37. C. M. Park, J. H. Kim, H. Kim and H. J. Sohn, *Chem. Soc. Rev.*, 2010, **39**, 3115-3141.
38. A. R. Kamali and D. J. Fray, *Rev. Adv. Mater. Sci.*, 2011, **27**, 14-24.
39. X. Wang, X. Cao, L. Bourgeois, H. Guan, S. Chen, Y. Zhong, D. M. Tang, H. Li, T. Zhai, L. Li, Y. Bando and D. Golberg, *Adv. Func. Mater.*, 2012, **22**, 2682-2690.
40. J. Lin, Z. Peng, C. Xiang, G. Ruan, Z. Yan, D. Natelson and J. M. Tour, *ACS Nano*, 2013, **7**, 6001–6006.
41. B. Luo, Y. Fang, B. Wang, J. Zhou, H. Song and L. Zhi, *Energy Environ. Sci.*, 2012, **5**, 5226-5230.
42. L. Mei, C. Xu, T. Yang, J. Ma, L. Chen, Q. Li and T. Wang, *J. Mater. Chem. A*, 2013, **1**, 8658-8664.
43. J. Zai, K. Wang, Y. Su, X. Qian and J. Chen, *J. Power Sources*, 2011, **196**, 3650-3654.
44. L. Y. Yeh and K. W. Cheng, *J. Power Sources*, 2015, **275**, 750-759.
45. F. Chen, J. Zai, M. Xu and X. Qian, *J. Mater. Chem. A*, 2013, **1**, 4316-4323.
46. Y. S. Yaşar, S. Kahraman, S. Çetinkaya and İ. Bilican, *J. Alloys Compd.*, 2015, **618**, 217-221.
47. J. Chen, L. Xu, W. Li and X. Gou, *Adv. Mater.*, 2005, **17**, 582-586.
48. H. Li, Z. Wang, L. Chen and X. Huang, *Adv. Mater.*, 2009, **21**, 4593-4607.
49. H. T. Tan, X. Rui, Z. Lu, C. Xu, W. Liu, H. H. Hng and Q. Yan, *J. Phys. Chem. C*, 2014, **118**, 17452-17460.
50. K. Chang and W. Chen, *ACS Nano*, 2011, **5**, 4720-4728.
51. B. Wu, H. Song, J. Zhou and X. Chen, *Chem. Commun.*, 2011, **47**, 8653-8655.
52. Q. Wang, L. Jiao, Y. Han, H. Du, W. Peng, Q. Huan, D. Song, Y. Si, Y. Wang and H. Yuan, *J. Phys. Chem. C*, 2011, **115**, 8300-8304.
53. W. W. Xiong, E. U. Athresh, Y. T. Ng, J. F. Ding, T. Wu and Q. C. Zhang, *J. Am. Chem. Soc.*, 2013, **135**, 1256-1259.
54. W. W. Xiong, P. Z. Li, T. H. Zhou, A. L. Y. Tok, R. Xu, Y. L. Zhao and Q. C. Zhang, *Inorg. Chem.*, 2013, **52**, 4148-4150.
55. W. W. Xiong, J. W. Miao, P. Z. Li, Y. L. Zhao, B. Liu and Q. C. Zhang, *Crystengcomm.*, 2014, **16**, 5989-5992.
56. W. W. Xiong, J. W. Miao, K. Q. Ye, Y. Wang, B. Liu and Q. C. Zhang, *Angew. Chem. Int. Ed.*, 2015, **54**, 546-550.
57. G. D. Zhang, P. Z. Li, J. F. Ding, Y. Liu, W. W. Xiong, L. N. Nie, T. Wu, Y. L. Zhao, A. I. Y. Tok and Q. C. Zhang, *Inorg. Chem.*, 2014, **53**, 10248-10256.
58. L. N. Nie, W. W. Xiong, P. Z. Li, J. Y. Han, G. D. Zhang, S. M. Yin, Y. L. Zhao, R. Xu and Q. C. Zhang, *J. Solid State Chem.*, 2014, **220**, 118-123.
59. X. Ji, K. T. Lee and L. F. Nazar, *Nat. Mater.*, 2009, **8**, 500-506.
60. X. Rui, J. Zhu, D. Sim, C. Xu, Y. Zeng, H. H. Hng, T. M. Lim and Q. Yan, *Nanoscale*, 2011, **3**, 4752-4758.
61. Y. Yu, C. H. Chen and Y. Shi, *Adv. Mater.*, 2007, **19**, 993-997.
62. M. S. Whittingham, Y. Song, S. Lutta, P. Y. Zavalij and N. A. Chernova, *J. Mater. Chem.*, 2005, **15**, 3362-3375.
63. N. Marx, L. Croguennec, D. Carlier, L. Bourgeois, P. Kubiak, F. d. r. L. Cras and C. Delmas, *Chem. Mat.*, 2010, **22**, 1854-1861.
64. M. S. Kishore, V. Pralong, V. Caignaert, U. V. Varadaraju and B. Raveau, *J. Power Sources*, 2007, **169**, 355-360.
65. G. M. Sheldrick, *SHELXS97 and SHELXL97*, University of Göttingen, Germany, 1997.
66. D. Y. Chung, T. Hogan, P. Brazis, M. Rocci-Lane, C. Kannewurf, M. Bastea, C. Uher and M. G. Kanatzidis, *Science*, 2000, **287**, 1024-1027.
67. A. Stein, S. W. Keller and T. E. Mallouk, *Science*, 1993, **259**, 1558-1564.
68. W. W. Xiong, J. R. Li, B. Hu, B. Tan, R. F. Li and X. Y. Huang, *Chem. Sci.*, 2012, **3**, 1200-1204.
69. W. W. Xiong, G. D. Zhang and Q. C. Zhang, *Inorg. Chem. Front.*, 2014 **1**, 292-300.
70. Q. C. Zhang, Y. Liu, X. H. Bu, T. Wu and P. Y. Feng, *Angew. Chem. Int. Ed.*, 2008, **47**, 113-116.
71. Q. Zhang, I. Chung, J. I. Jang, J. B. Ketterson and M. G. Kanatzidis, *J. Am. Chem. Soc.*, 2009, **131**, 9896-9897.
72. H. Y. Lin, C. Y. Chin, H. L. Huang, W. Y. Huang, M. J. Sie, L. H. Huang, Y. H. Lee, C. H. Lin, K. H. Lii, X. H. Bu and S. L. Wang, *Science*, 2013, **339**, 811-813.
73. Z. Y. Zhang, J. Zhang, T. Wu, X. H. Bu and P. Y. Feng, *J. Am. Chem. Soc.*, 2008, **130**, 15238-15239.
74. R. C. Zhang, H. G. Yao, S. H. Ji, M. C. Liu, M. Ji and Y. L. An, *Inorg. Chem.*, 2010, **49**, 6372-6374.
75. R. C. Zhang, C. Zhang, S. H. Ji, M. Ji and Y. L. An, *J. Solid State Chem.*, 2012, **186**, 94-98.
76. R. C. Zhang, H. G. Yao, S. H. Ji, M. C. Liu, M. Ji and Y. L. An, *Chem. Commun.*, 2010, **46**, 4550-4552.
77. B. Qu, M. Zhang, D. Lei, Y. Zeng, Y. Chen, L. Chen, Q. Li, Y. Wang and T. Wang, *Nanoscale*, 2011, **3**, 3646-3651.
78. Z. Du, S. Zhang, J. Zhao, T. Jiang and Z. Bai, *Int. J. Electrochem. Sci.*, 2012, **7**, 1180-1186.
79. L. Huang, H. B. Wei, F. S. Ke, X. Y. Fan, J. T. Li and S. G. Sun, *Electrochimica Acta*, 2009, **54**, 2693-2698.
80. I. Amadei, S. Panero, B. Scrosati, G. Cocco and L. Schiffini, *J.Power Sources*, 2005, **143**, 227-230.
81. J. Yang, Y. Zhang, C. Sun, G. Guo, W. Sun, W. Huang, Q. Yan and X. Dong, *J. Mater. Chem. A*, 2015, **3**, 11462-11470.